Preparation of a γ-Alumina Film Doped with Fine γ-Iron(III) Oxide Particles

Yoshio Kobayashi, Dai Kawashima, and Akira Tomita*

Institute for Chemical Reaction Science, Tohoku University, Katahira, Aoba-ku, Sendai 980-77, Japan

Received March 19, 1997. Revised Manuscript Received May 28, 1997[⊗]

A poly(vinyl alcohol)−alumina hydrate composite film prepared by using a sol−gel process was transparent in the visible region. The composite film was insoluble in water after being heated at about 100 °C but exhibited hydrophilicity. These characteristics are suitable for the deposition of $Fe_2O_3 \cdot nH_2O$ in the film by a counter diffusion method. By heating at 600 °C in air, this deposited film was transformed to a γ-Fe_2O_3-doped γ-Al_2O_3 film. No absorption peaks were observed in the visible region at a wavelength of >550 nm. The crystallite size could be controlled in the range 3−8 nm by changing the counter diffusion time. Due to the orientation of the alumina hydrate matrix, the γ-Fe_2O_3-doped film was more easily magnetized in the direction parallel to the film plane than to the perpendicular.

Introduction

It is well-known that the physical properties of nanoscale materials, such as semiconductor, metal, and magnetic materials, are quite different from those of the bulk materials.[1−3] Therefore, the minimization of the particle size of iron oxide, which is one of the most widely used magnetic materials, is a challenging research subject. However, such fine particles are not stable, and they tend to easily aggregate. This difficulty is circumvented by dispersing fine particles into a solid matrix. To prepare fine particle-doped materials, melting,[4,5] sol−gel,[6,7] and sputtering methods[8−10] have been proposed so far. In the melting method, doped materials are prepared by melting the dopant and matrix and then cooling the molten mixture. With this method, it is difficult to freely select the combination of dopant and matrix, and the concentration of the dopant in the matrix is limited. Furthermore, defects are easily produced in fine particles. The sol−gel method is simple, but various species derived from the raw materials and/or hydrolysis catalyst remain in the product. The sputtering method requires special apparatus, but any pair of dopant and matrix can be used and no species besides dopant and matrix remains in the product. In addition to these methods, Kurokawa proposed a "counter diffusion method", which allows the dispersion of various types of materials in a matrix by using a simple apparatus.[11] In this study, we applied the counter diffusion method to disperse fine iron oxide particles in an alumina matrix.

The counter diffusion method requires the matrix to be hydrophilic as well as insoluble in water. Therefore, organic polymers such as cellulose acetate and cross-linked poly(vinyl alcohol) (PVA) have been often used as a matrix in this method. Such films, however, are not thermally stable and thereby cannot be used at high temperatures. Inorganic materials, which are thermally stable compared to organic polymers, would be the best matrix. There are, however, few inorganic materials which have both hydrophilicity and water insolubility. Instead, a nanocomposite of an inorganic material and hydrophilic organic polymer can be used as a matrix for this method. This type of nanocomposite has been made by several researchers using a sol−gel process.[12−22] The preparation of a PVA−alumina hydrate composite by the sol−gel method has been reported by Suzuki et al.,[21] who, however, did not investigate the behavior of the composite in water.

The final objective of this study is to establish a new and simple method for the doping of fine particles into an inorganic matrix. In the present study, we prepared a PVA−alumina hydrate nanocomposite by the sol−gel method and investigated its properties in water. Then,

* To whom all correspondence should be addressed. E-mail: tomita@icrs.tohoku.ac.jp.

[⊗] Abstract published in *Advance ACS Abstracts,* July 15, 1997.

(1) Brus, L. *J. Phys. Chem.* **1986**, *90*, 2555.
(2) Ekimov, A. I.; Efros, Al. L.; Onushchenko, A. A. *Solid State Commun.* **1993**, *88*, 947.
(3) Kimura, K. *Z. Phys. D* **1989**, *11*, 327.
(4) Borrelli, N. F.; Hall, D. W.; Holland, H. J.; Smith, D. W. *J. Appl. Phys.* **1987**, *61*, 5399.
(5) Ekimov, A. I.; Efros, AI. L.; Onushchenko, A. A. *Solid State Commun.* **1985**, *56*, 921.
(6) Nogami, M.; Nagasaka, K.; Kato, E. *J. Am. Ceram. Soc.* **1990**, *73*, 2097.
(7) Minti, H.; Eyal, M.; Reisfeld, R.; Berkovic, G. *Chem. Phys. Lett.* **1991**, *183*, 277.
(8) Potter, Jr. B. G.; Simmons, J. H. *Phys. Rev. B* **1988**, *37*, 10838.
(9) Tsunetomo, K.; Nasu, H.; Kitayama, H.; Kawabuchi, A.; Osaka, Y.; Takiyama, K. *Jpn. J. Appl. Phys.* **1989**, *28*, 1928.
(10) Tanahashi, I.; Tsujimura, A.; Mitsuyu, T.; Nishino, A. *Jpn. J. Appl. Phys.* **1990**, *29*, 2111.
(11) Kurokawa, Y. *Desalination* **1982**, *41*, 115.
(12) Hino, T.; Mochida, K.; Okamura, S. *Kobunshi Ronbunshu* **1983**, *40*, 225.
(13) Ikoma, S.; Nomoto, E.; Yokoi, H. *Kobunshi Ronbunshu* **1991**, *48*, 53.
(14) Stefanithis, I. D.; Mauritz, K. A. *Macromolecules* **1990**, *23*, 2397.
(15) Kohjiya, S.; Ochiai, K.; Yamashita, S. *J. Non-Cryst. Solids* **1990**, *119*, 132.
(16) Schmidt, H. *J. Non-Cryst. Solids* **1985**, *73*, 681.
(17) Chujo, Y.; Matsuki, H.; Kure, S.; Saegusa, T.; Yazawa, T. *J. Chem. Soc., Chem. Commun.* **1994**, 635.
(18) Toki, M.; Chow, T. Y.; Ohnaka, T.; Samura, H.; Saegusa, T. *Polym. Bull.* **1992**, *29*, 653.
(19) Huang, H.-H.; Wilkes, G. L.; Carlson, J. G. *Polymer* **1989**, *30*, 2001.
(20) Mark, J. E.; Sun, C.-C. *Polym. Bull.* **1987**, *18*, 259.
(21) Suzuki, F.; Onozato, K.; Kurokawa, Y. *J. Appl. Polym. Sci.* **1990**, *39*, 371.
(22) Coltrain, B. K.; Landry, C. J. T.; O'Reilly, J. M.; Chamberlain, A. M.; Rakes, G. A.; Sedita, J. S.; Kelts, L. W.; Landry, M. R.; Long, V. K. *Chem. Mater.* **1993**, *5*, 1445.

S0897-4756(97)00157-9 CCC: $14.00

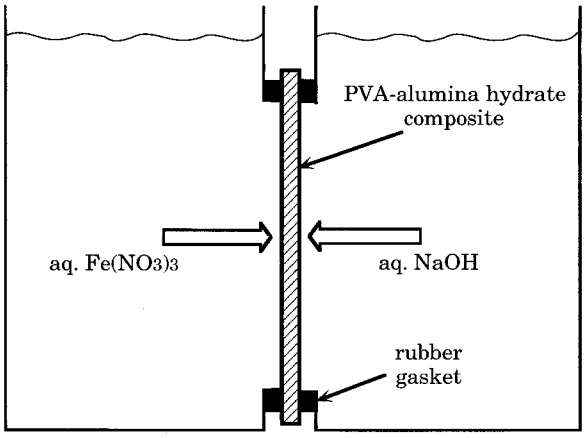

Figure 1. Schematic diagram of the counter diffusion apparatus.

we attempted to disperse iron hydroxide fine particles into the composite by using the counter diffusion method and to prepare iron oxide-doped alumina by calcining the iron hydroxide-doped composite in air.

Experimental Section

Sample Preparation. An alumina sol was prepared by the method reported by Yoldas.[23] Aluminum triisopropoxide was hydrolyzed with water. The molar ratio of water to alkoxide was 100:1. After heating at 80 °C under stirring for 1 h, the mixture became slurry. Then, acetic acid was added to the slurry at a molar ratio of acetic acid to alkoxide of 0.15:1. In 8 h, the mixture became a transparent sol. By using this sol, a transparent PVA−alumina hydrate composite film was prepared by the method reported by Suzuki et al.[21] A 5 wt % aqueous solution of PVA was added to the alumina sol, the amount of PVA and alumina being equal by weight. The mixture was spread on a flat polystyrene petri dish and dried in air at room temperature. A PVA−alumina hydrate composite film was obtained after gelation. The gelation took 3 days. The film was then heated in air at various temperatures between 60 and 120 °C to investigate the effect of heat treatment temperature on its properties. For comparison, alumina hydrate and PVA films were separately prepared by gelation of the alumina sol and aqueous PVA, respectively.

When the composite film was placed into water, it became rubberlike. The composite was doped with iron hydroxide by using a counter diffusion method.[11] Figure 1 shows a schematic diagram of the apparatus, which has two containers separated by the composite film. Aqueous $Fe(NO_3)_3$ (0.1 mol/L) and aqueous NaOH (0.1 mol/L) were placed into the respective containers. Fe^{3+} and OH^- ions diffused countercurrently and contacted inside of the film, and then an $Fe_2O_3 \cdot nH_2O$ precipitate was deposited. The diffusion time was 1, 3, and 6 h. After washing with water, the resultant film was heated at 600 °C in air to burn out the PVA. Thus, an Fe_2O_3-doped Al_2O_3 film was obtained.

Sample Characterization. Dynamic light-scattering measurements were carried out with a laser particle analyzer (Ohtsuka Electronics DLS-7000).

The morphology of the film was observed by scanning electron microscopy (SEM). For SEM analysis, a small fragment of the film was fixed on an Al stage by Ag paste and then Pt/Pd was sputtered onto its surface. SEM analysis was carried out by using a Hitachi Model S-900 operating at an accelerating voltage of 15 kV.

For transmission electron microscopy (TEM) analysis, the film was pulverized and suspended in ethanol. The suspension was dropped onto a TEM microgrid. TEM photographs were taken by a JEOL Model JEM-3010 operating at an accelerating voltage of 300 kV.

(23) Yoldas, B. E. *Am. Ceram. Soc. Bull.* **1975**, *54*, 286.

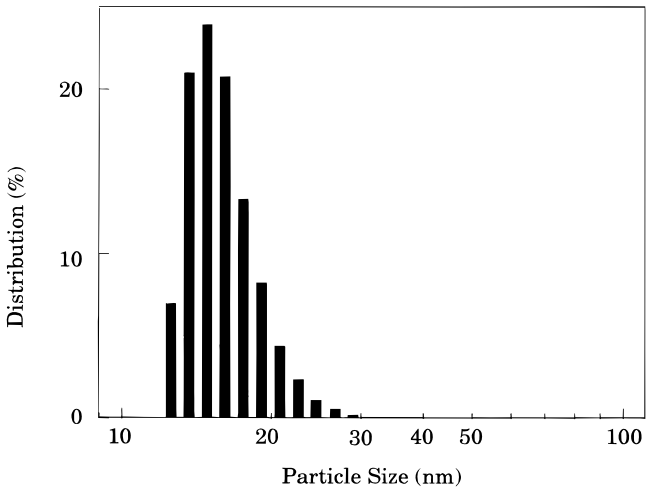

Figure 2. Particle size distribution of alumina sol.

The intact film with a thickness of about 0.1 mm was examined with ultraviolet (UV) and visible (vis) absorption spectra. They were recorded on a Hitachi U-3500 photometer.

The surface areas of films were determined by the BET method making use of N_2 gas adsorption isotherms. The isotherms were recorded on a Quantachrome Model Autosorb-1.

The water absorption ability and water solubility of the composite film were determined as follows. The composite film with a weight of W_0 was put into water for 1 h. The weight of wet film, W_1, was measured immediately after being taken out of water. The weight decreased to W_2 after drying at 40 °C for 24 h. The amount of water absorbed in the film is $W_1 - W_2$, while the amount of the composite dissolved in water is $W_0 - W_2$. The water absorption ability and the water solubility are defined as follows:

$$\text{water absorption ability} = (W_1 - W_2)/W_2 \quad (1)$$

$$\text{water solubility} = (W_0 - W_2)/W_0 \quad (2)$$

The properties of PVA itself in water were determined in a similar manner.

The content of iron oxide was determined by inductively coupled plasma (ICP) analysis. The iron oxide-doped alumina film, about 20 mg, was dissolved in 1 mL of aqueous hydrofluoric acid. Boric acid powder (5 g) was added to this solution for neutralization. ICP analysis of the resultant solution was carried out by using a Shimadzu Model ICPS 1000 III spectrometer.

X-ray diffraction (XRD) patterns were recorded by a Shimadzu XD-D1 instrument operated at 30 kV and 20 mA with Cu Kα radiation and Ni filter. Both intact film and powder were examined.

Infrared (IR) spectra of the intact films were recorded on a Shimadzu FTIR-8100-M Fourier transform infrared spectrophotometer in the range 500−4600 cm^{-1}.

Thermogravimetry and differential thermal analysis were carried out in air with a Shinka-Riko TG-7000 instrument at a heating rate of 10 °C/min.

Magnetization was measured by a TOEI VSM-3 vibrating sample magnetometer with 50 Hz vibrating frequency and a magnetic field up to 10 kOe at room temperature. The sample film was set perpendicular or parallel to the magnetic field.

Results and Discussion

PVA−Alumina Hydrate Composite Film. Figure 2 shows the particle size distribution of the transparent alumina sol determined by the light-scattering method. The size of the sol particles is in the range 13−30 nm. Its mixture with aqueous PVA was slowly dehydrated at room temperature to form the PVA−alumina hydrate composite film. This film is transparent without any

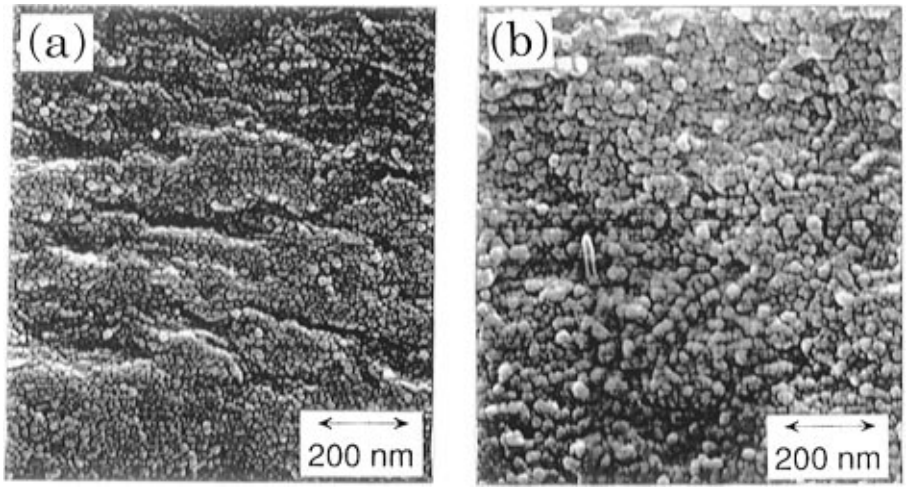

Figure 3. SEM photographs of the cross sections of films. (a) Alumina hydrate film; (b) PVA−alumina hydrate composite film.

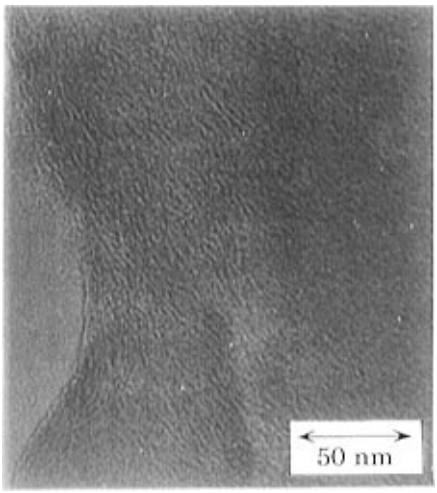

Figure 4. TEM photograph of PVA−alumina hydrate film.

turbidity. Its UV−vis transmission spectrum shows that the composite film was transparent in the range 340−700 nm (this spectrum is presented later as a part of Figure 8). It was more flexible than the alumina hydrate film containing no PVA. Figure 3 shows SEM photographs of the alumina hydrate and PVA−alumina hydrate films. These surfaces correspond to the broken surfaces of the films obtained by applying a bending stress. Many round homogeneous particles were observed with sizes of about 10 nm for the alumina hydrate and about 20 nm for the PVA−alumina hydrate films, respectively. The particle sizes in the alumina hydrate are in agreement with those of the alumina sol. The particles in the composite film are somewhat larger. The surface areas of the alumina hydrate and the PVA−alumina hydrate film were determined as 310 and 7 m^2/g, respectively. It is thought that PVA fills the pores of the alumina hydrate, thereby making the composite film less porous. Thus, PVA and alumina hydrate were combined at the nanoscale by the sol−gel method. Figure 4 shows a TEM photograph of the PVA−alumina hydrate film. This also shows the uniform hybridization of the inorganic and organic components.

Figure 5 shows the XRD patterns of the PVA−alumina hydrate composite film, together with the patterns of PVA and alumina hydrate. All the peaks of the composite are attributed to PVA or boehmite. The relative intensity of the peak at 14° of the composite

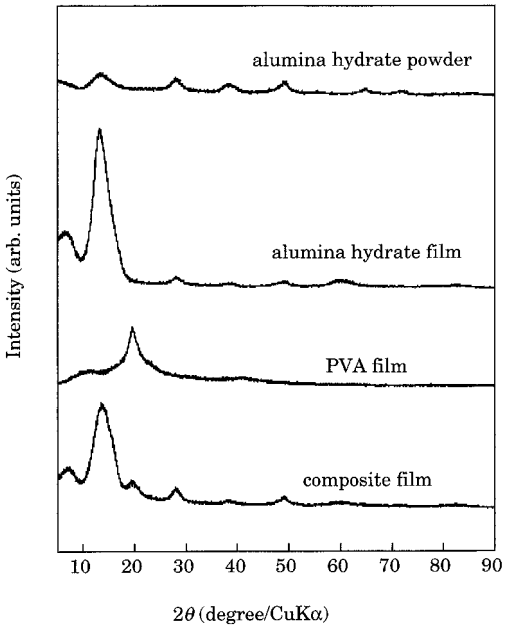

Figure 5. X-ray diffraction patterns of alumina hydrate, PVA film, and PVA−alumina hydrate composite film.

Table 1. Effect of Heat Treatment Temperature on the Water Absorption Ability and Solubility of PVA Film and PVA−Alumina Hydrate Film

heat treatment temperature (°C)	water absorption ability (g/g)		solubility in water (g/g)	
	PVA	PVA/Al_2O_3	PVA	PVA/Al_2O_3
no heat treatment		11.1		0.06
80	4.4	3.4	0.084	0.023
100	3.1	1.2	0.052	0.005
120	1.9	0.6	0.021	0.003

film, which can be attributed to a (020) reflection of boehmite, is larger than that of the alumina hydrate powder. This indicates that the alumina hydrate in the composite had a preferred orientation with the boehmite (020) plane parallel to the film plane. Similar results were reported by Wakakuwa et al.[24] and Pierre et al.[25]

Table 1 shows the dependence of the water absorption ability of the composite film on the heat treatment

(24) Wakakuwa, M.; Kawashima, M.; Makishima, A. In *Proc. 4th Inter. Symp. Sci. Technol. Sintering, Tokyo, November 1987*; Somiya, D., et al., Eds.; Elsevier: London, 1988; Vol. 1, p 139.

(25) Pierre, A. C.; Uhlmann, D. R. *J. Am. Ceram. Soc.* **1987**, *70*, 28.

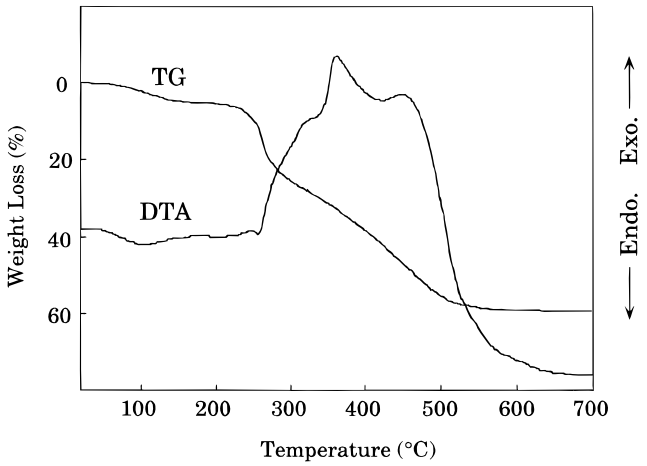

Figure 6. TG-DTA curves of PVA−alumina hydrate composite film in air.

temperature. For comparison, the result of PVA alone was indicated. The data for PVA without heat treatment were not presented in this table, because it dissolved in water and its absorption ability could not be measured. The absorption abilities of both the composite and PVA decreased as the heat treatment temperature increased. The water solubility of the composite as a function of heat treatment temperature is also presented in Table 1. A small amount of PVA was dissolved even after PVA was heat treated at 120 °C, whereas the solubility of the composite was almost negligible at above 100 °C. Thus the composite exhibits hydrophilicity and yet insolubility in water upon heat treatment at relatively low temperatures, such as 100 °C. The IR absorption was measured to determine the change upon composite formation. However, the change in the spectrum of the composite before and after heat treatment was not significant; most of the peaks for the composite were assigned either to PVA or to alumina hydrate. Thus, the IR data could not explain the hydrophilicity and water insolubility of the composite.

Figure 6 shows the TG-DTA curves for pulverized PVA−alumina hydrate. An exothermic weight decrease occurred in the range 250−600 °C. This weight loss corresponded to the weight of PVA. No weight loss was observed after 600 °C. Therefore, the heat treatment of the composite film at 600 °C ensures the complete transformation of the composite to an Al_2O_3 film which was transparent like the initial film. In the TEM photographs of the Al_2O_3 film (Figure 7a,b), the forma-

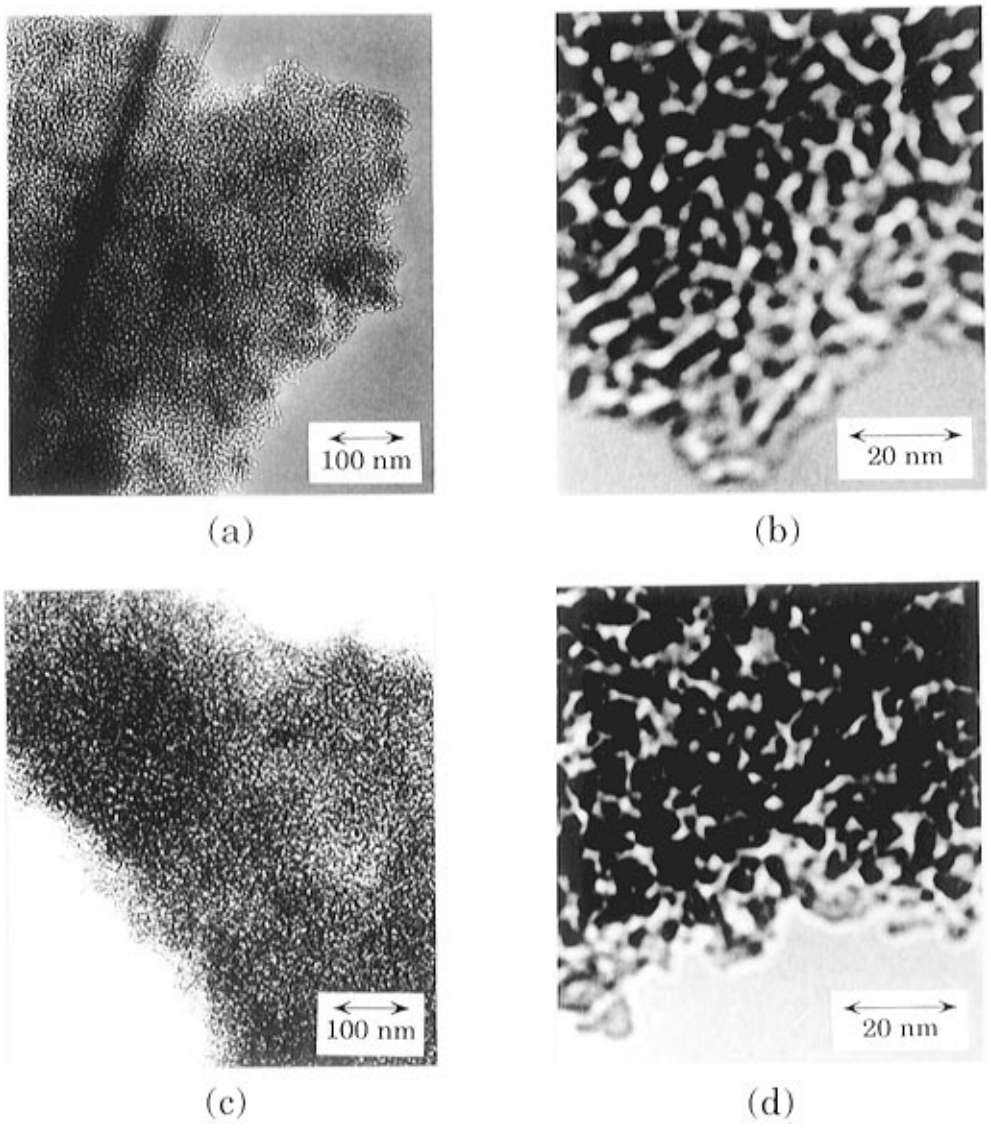

Figure 7. TEM photographs of nondoped alumina film (a and b) and iron oxide-doped alumina films with doping time, 6 h (c and d).

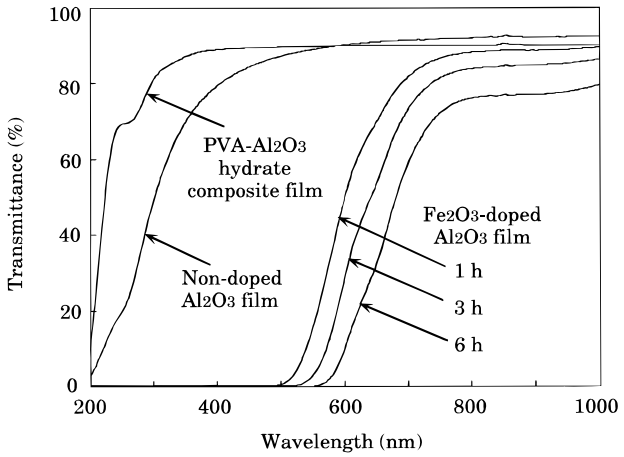

Figure 8. UV−vis absorption spectra of PVA−alumina hydrate film, nondoped alumina film, and iron oxide-doped alumina films with different doping times.

tion of an alumina gel network was observed. The Al_2O_3 film is less transparent than the PVA/alumina hydrate film (Figure 8). Since the former film was calcined at 600 °C, the formation of microvoids due to the volatilization of PVA is likely to increase the scattering and reduce the transparency of the film. It is also possible that the increase in the size of the alumina particles due to calcination results in the reduction of transparency, since in general, the larger the particle size, the less transparent in the UV range.

Alumina Film Containing Iron Oxide. The PVA−alumina hydrate composite film exhibits hydrophilicity but water insolubility as mentioned above. We doped the composite film with $Fe_2O_3 \cdot nH_2O$ by taking advantage of these unique properties. The $Fe_2O_3 \cdot nH_2O$−PVA−alumina hydrate film was brown. When the doped PVA−alumina hydrate film was calcined in air at 600 °C, which is high enough to burn off the PVA, an alumina film containing iron oxide was obtained. Figure 7c,d shows TEM photographs of the iron oxide-doped alumina films. The gel network patterns as observed in the nondoped alumina were less clear in the doped alumina. It seems that iron oxide particles were formed in the alumina gel network. However, it is impossible to obtain information on the morphology and size distribution of the iron oxide particles from the TEM analysis, because it is hard to discriminate the iron oxide particles from the alumina network. Because no particles of micron size were observed in the TEM photographs, it seems that the iron oxide particles exist in the doped film at the nanoscale. Figure 9 shows the XRD patterns of the doped films. For comparison, an XRD pattern of Al_2O_3 obtained by calcining PVA−alumina hydrate is also shown. The peaks at about 45° and 65° are attributed to γ-Al_2O_3. The peaks at about 30.5°, 35.8°, 57.5°, and 63.3° are due to the (220), (311), (511), and (440) reflections of γ-Fe_2O_3. Thus, $Fe_2O_3 \cdot nH_2O$ was transformed to γ-Fe_2O_3. The average crystallite size of the γ-Fe_2O_3 was estimated from X-ray diffraction line broadening of the (311) peak according to the Scherrer equation; the size was 3.0, 5.0, and 8.0 nm for the doping time of 1, 3, and 6 h, respectively. An X-ray microanalysis of the cross section of the doped Al_2O_3 film revealed that most of the iron oxide was present in the middle portion. The iron contents in the doped films were estimated by ICP analysis. The Fe_2O_3 contents

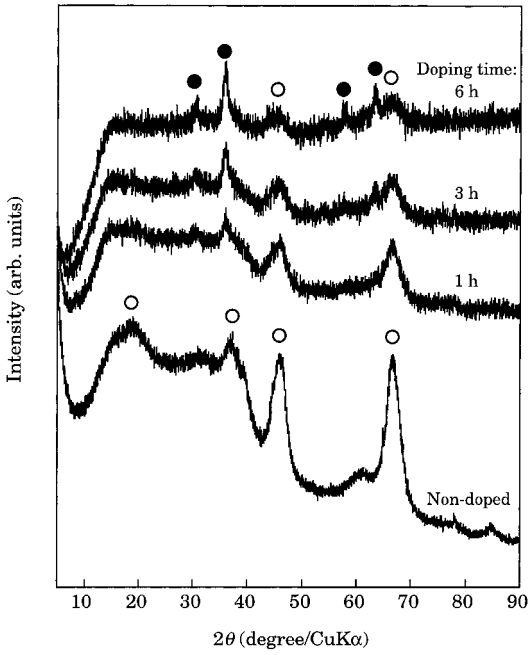

Figure 9. X-ray diffraction patterns of nondoped alumina film and iron oxide-doped alumina films with different doping times. (●) γ-Fe_2O_3, (○) γ-Al_2O_3.

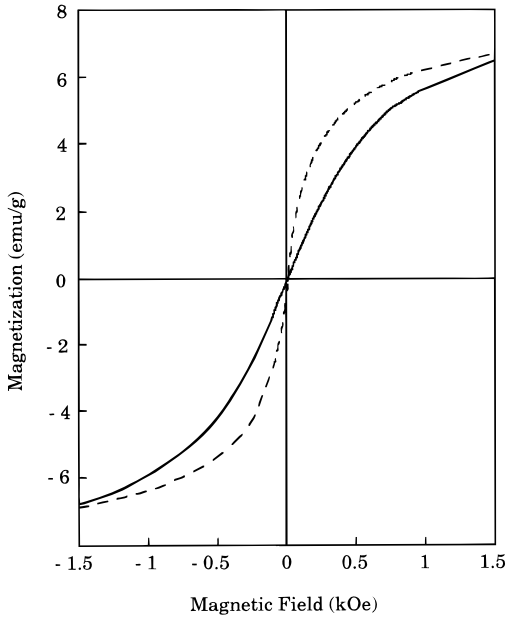

Figure 10. Magnetization curves of Fe_2O_3-doped alumina film with a doping time of 6 h. Magnetic field were perpendicular (solid line) and parallel (dotted line) to the film plane.

were determined as 6.5, 12.1, and 24.7 wt % for doping times of 1, 3, and 6 h, respectively. The UV−vis spectra of the Fe_2O_3-doped Al_2O_3 films are shown on the right hand side of Figure 8. The size of the γ-Fe_2O_3 was so small that the films allow the transmission of a substantial fraction of the visible light. With an increase in the doping time, the absorption edge shifted to longer a wavelength because of the size effect.[26]

Figure 10 shows the magnetization curve for the Fe_2O_3-doped film. The film set parallel to the magnetic field has a steeper slope in the portion of the initial magnetization range than does the perpendicular one, indicating that the film is easier to magnetize parallel

(26) Brus, L. E. *J. Chem. Phys.* **1984**, *80*, 4403.

Table 2. Saturation Magnetization of Iron Oxide-Doped Alumina Films

doping time (h)	Fe_2O_3 content (wt %)	M_S (emu/g of film)	M_S (emu/g of Fe_2O_3)
1	6.5	1.2	18.6
3	12.1	3.0	24.7
6	24.7	8.8	35.7

to the film plane. In other words, the doped film exhibited a magnetic anisotropy. The alumina hydrate in the PVA−alumina hydrate composite film has a preferred orientation of the (020) planes parallel to the film plane (Figure 5). It is thought that this orientation controls the direction of crystal growth of the $Fe_2O_3 \cdot nH_2O$, and thereby, the crystal growth direction of the γ-Fe_2O_3 fine particles became parallel to the film plane. The saturation magnetization values of two settings were almost the same. The observed saturation magnetizations, M_S, are shown in Table 2 in terms of both film weight basis and iron oxide weight basis. Ms increased with the content of Fe_2O_3, but it was always lower than the saturation magnetization of bulk γ-Fe_2O_3 crystal, about 70 emu/g. This indicates the possibility that a part of iron oxide in Al_2O_3 is not γ-Fe_2O_3.

Conclusions

The unique property of PVA−alumina hydrate composite films, hydrophilicity and insolubility in water, enabled us to prepare an $Fe_2O_3 \cdot nH_2O$-doped film. A γ-Fe_2O_3-doped γ-Al_2O_3 film could then be prepared by heat treating the above film at 600 °C in air. The crystallite size of γ-Fe_2O_3 was 3−8 nm, and this film showed an anisotropic magnetization behavior.

Acknowledgment. The present authors express their thanks to Associate Professor Sumiyama at the Institute for Materials Research, Tohoku University, for magnetic measurements.

CM970157Z